Influence of Polyoxovanadate and Phthalocyanine on 4f Electron Transfer in Gold-Confined Monolayers Probed with EGaIn Top Contacts

Soni, Saurabh; Werner, Irina; Aidi, Michael; Moors, Marco; Mthembu, C. Lungani; Zharnikov, Michael; Havenith, Remco W.A.; Monakhov, Kirill Yu.; Chiechi, Ryan C.

Published in:
ACS Applied Nano Materials

DOI:
10.1021/acsanm.3c05021

Publication date:
2023

ACS APPLIED NANO MATERIALS

www.acsanm.org Letter

Influence of Polyoxovanadate and Phthalocyanine on 4f Electron Transfer in Gold-Confined Monolayers Probed with EGaIn Top Contacts

Saurabh Soni, Irina Werner, Michael Aidi, Marco Moors, C. Lungani Mthembu, Michael Zharnikov, Remco W. A. Havenith, Kirill Yu. Monakhov,* and Ryan C. Chiechi*

Cite This: *ACS Appl. Nano Mater.* 2023, 6, 22643−22650 Read Online

ACCESS | Metrics & More | Article Recommendations | Supporting Information

ABSTRACT: This work describes the effects of dodecavanadate anions and phthalocyanine ligands as well as the identity of lanthanide centers on the charge transport characteristics of heterometallic complexes $(nBu_4N)_3[HV_{12}O_{32}Cl(LnPc)]$ and $(nBu_4N)_2[HV_{12}O_{32}Cl(LnPc)_2]$ for Sm^{III}−Er^{III}, Lu^{III}, and Y^{III} on gold surfaces. In molecular ensemble junctions with eutectic Ga−In top contacts, the complexes containing two phthalocyanine ligands are highly conductive but show no clear effect of varying the lanthanide. By contrast, the complexes that omit phthalocyanine but include 4f-functionalized dodecavanadate building blocks show clear trends in conductance, rectification, and transition voltages. Density functional theory calculations show that the occupied and unoccupied frontier orbitals in the heterometallic complexes are delocalized on the phthalocyanine ligand and dodecavanadate anion, respectively, suggesting strong lanthanide−ligand electronic coupling. Near-edge X-ray absorption fine structure spectroscopy on these complexes further suggests that the phthalocyanine ligands are arranged such that their edges are in contact with the electrodes, creating tunneling transmission channels that bypass the lanthanide, effectively obviating the electronic contributions of the lanthanide centers to charge transport. These results separate the influence of the individual constituents of these metal−ligand complexes on the tunneling charge-transport properties. These results demonstrate how strongly coupled ligands such as phthalocyanine can dominate charge transport, from which we construct design rules for harnessing the properties of f-block elements in redox-active molecular heterojunctions.

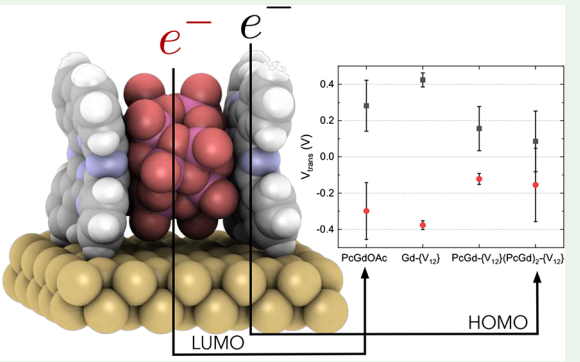

KEYWORDS: *EGaIn, Polyoxometalate, Molecular electronics, Vanadium, Lanthanide, Scanning probe methods*

INTRODUCTION

Research in molecular electronics aims to explore new ways to fabricate next-generation electronic devices with individual molecules, mitigating charge transport. Applications for such devices include emerging technologies such as neuromorphic, biocompatible, wearable, and flexible electronics.[1−3] The bottom-up fabrication of two-dimensional molecular ensemble junctions (MEJs) comprising self-assembled monolayers (SAMs)[2] is the most direct route to these molecule-based electronic applications. Polyoxometalate (POM) compounds designed to form robust SAMs[4,5] offer a unique molecular platform for pursuing these goals. The relative ease of systematically augmenting POMs toward inorganic−organic hybrid structures of interest is beneficial for tailoring the POM reactivity on substrate surfaces via the ligand functionality and of the corresponding charge-transfer properties.[6−9] The self-assembly of molecules on surfaces is governed by the specific interactions between molecules and the chemistry at their interface and POMs are no exception; their organization, orientation, stability, reactivity, and redox activity depend strongly on the properties of the substrate[10] (e.g., hydrophobic vs hydrophilic[11]) and its passivation/functionalization.[12−14] It can also be influenced by methods of molecular deposition[6,15] and the adsorption of POM itself can exert electronic effects on, e.g., biomolecular nanostructures such as DNA origami confined to the surface.[16] The utility of POMs as redox-active building blocks includes the investigation of electron transport in the context of polarizability,[17] spintronics,[18,19] organic neuromorphics,[20−22], thermoelectrics,[23] molecular magnetism,[24,25] molecular sensors,[26] and plasmonics.[27,28] Thus, POMs are a natural extension of molecular electronics[4,9,29]

Received: October 20, 2023
Revised: November 17, 2023
Accepted: December 5, 2023
Published: December 7, 2023

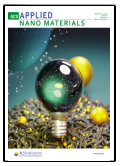

https://doi.org/10.1021/acsanm.3c05021
ACS Appl. Nano Mater. 2023, 6, 22643−22650

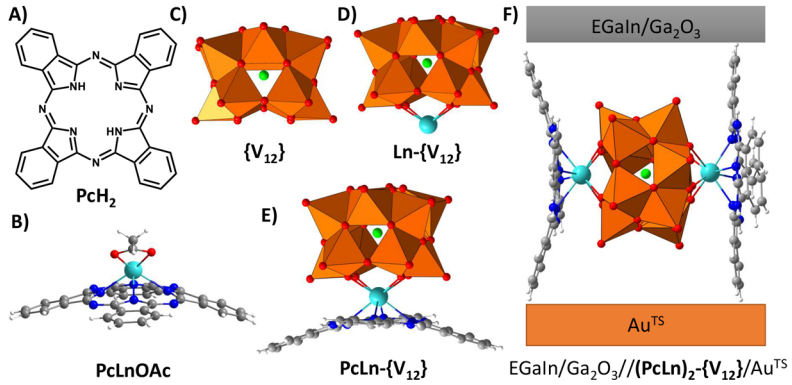

Figure 1. Molecular systems studied in this work: (A) phthalocyanine, PcH_2; (B) phthalocyanine-lanthanide complex, PcLnOAc; (C) polyoxovanadate, $\{V_{12}\}$; (D) lanthanide-polyoxovanadate complex, Ln-$\{V_{12}\}$; and phthalocyanine-lanthanide-polyoxovanadate complexes (E) PcLn-$\{V_{12}\}$ and (F) $(PcLn)_2$-$\{V_{12}\}$, shown as an idealized structure inside a MEJ. Color code: VO_5 polyhedra are orange; O = red; Cl = green; Ln = aqua; C = dark gray; N = blue; H = white. Solvent ligands (in the case of Ln-$\{V_{12}\}$ and PcLnOAc), countercations (in all examples, except for PcH_2 and PcLnOAc), and H atoms at the $\{V_{12}\}$ cage are not shown.

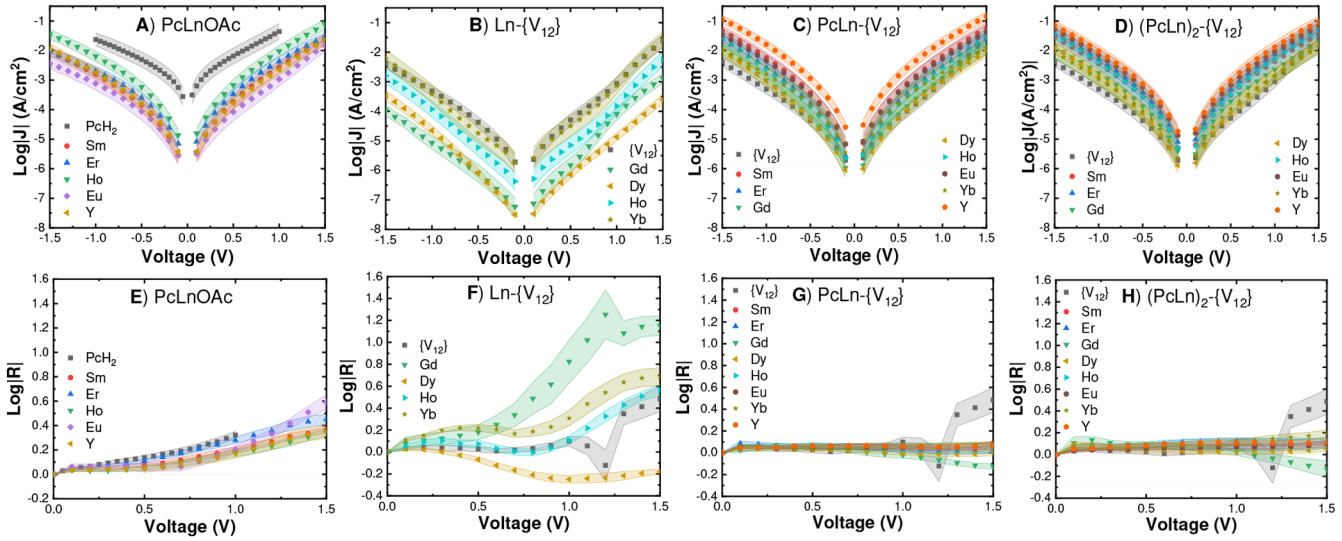

Figure 2. Semilog plots of current density ($\log |J/(A/cm^2)|$) and rectification ratio ($\log |R|$) vs the applied voltage (V) for the following: (A and E) PcLnOAc and PcH_2; (B and F) Ln-$\{V_{12}\}$ and $\{V_{12}\}$; (C and G) PcLn-$\{V_{12}\}$ and $\{V_{12}\}$; (D and H) $(PcLn)_2$-$\{V_{12}\}$ and $\{V_{12}\}$. The error bars represent 95% confidence intervals. The mean values and confidence intervals were obtained from Gaussian fits to histograms by acquiring data from 3 to 4 samples per molecule, with 12 junctions per substrate and 5 forward and reverse scans per junction. These details are summarized in the Supporting Information and Table S2.

into the phenomenology of f-shell lanthanides[24,30−34] and their interactions with transition metals, metal−ligand charge transfer effects, shielding effects, and other potentially useful, yet-to-be-discovered electron charge and spin phenomena at the nanoscale.[35]

Previously, we reported polyoxovanadate (POV) complexes covalently functionalized with one or two phthalocyaninato-Yb groups, namely, $[V_{12}O_{32}Cl(YbPc)_n]^{n-5}$ $n = \{1, 2\}$.[36] These complexes were shown to form remarkably stable and robust SAMs readily on template-stripped Au (Au^{TS}) substrates[37] exhibiting stable electrical characteristics in tunneling junctions with top contacts of eutectic gallium−indium (EGaIn) metal alloy.[38] We subsequently synthesized isostructural $(nBu_4N)_3[HV_{12}O_{32}(Cl)](LnPc)$ and $(nBu_4N)_2[HV_{12}O_{32}(Cl)](LnPc)_2$ (hereafter referred to as PcLn-$\{V_{12}\}$ and $(PcLn)_2$-$\{V_{12}\}$, respectively), extending the range of rare earths from early to late lanthanides (Sm^{III}−Er^{III}, Lu^{III}, and Y^{III}).[39] These hybrid compounds exhibited not only remarkable intramolecular charge transfer and redox-induced magnetism but also unusual intermolecular communication via a complex interplay of the POVs, Pc, Ln, and countercation units.

In the current work, we incorporate our $\{V_{12}\}$-type POVs as axial ligands in conjunction with macrocyclic lanthanide complexes LnPc in MEJs to understand the mechanism of action of these electron-transport molecular materials regarding the role of lanthanides and POV countercations[8,40,41] on conducting surfaces (specifically, Au). We describe physical levers that control the charge-transport characteristics of responsive SAMs built upon the covalent functionalization of POVs by LnPc moieties and compare the data to SAMs of their precursor compounds. The compounds investigated herein are shown in Figure 1: (i) metal-free phthalocyanine (PcH_2); (ii) lanthanide phthalocyanine acetate complexes PcLnOAc·MeOH·H_2O[36,39,42] with Ln = Sm^{III}−Er^{III}, Yb^{III}, and Y^{III} (abbreviated as PcLnOAc); (iii) the dodecavanadate

https://doi.org/10.1021/acsanm.3c05021
ACS Appl. Nano Mater. 2023, 6, 22643−22650

$(nBu_4N)_4[HV_{12}O_{32}Cl]$[43] (abbreviated as $\{V_{12}\}$); (iv) $(nBu_4N)_2[LnV_{12}O_{32}(Cl)](H_2O)_2(CH_3CN)_2$[44] with Ln = Gd^{III}, Dy^{III}, Ho^{III}, Yb^{III} (abbreviated as Ln-$\{V_{12}\}$); as well as the hybrid compounds of interest (v) PcLn-$\{V_{12}\}$, and (vi) **(PcLn)$_2$-{V$_{12}$}** (with Ln = Sm^{III}–Gd^{III}, Dy^{III}–Er^{III}, Yb^{III} and Y^{III} in each case. The Y^{III} complexes were studied as controls with a nonlanthanide metal center.

RESULTS AND DISCUSSION

We grew SAMs of all of the Ln complexes discussed in the above paragraph (shown in Figure 1) by immersing atomically flat template-stripped[37] gold substrates (Au^{TS}) in 50 μM methanol solutions of the precursors, as we did with the aforementioned complexes.[36] We confirmed the immobilization of these complexes and the subsequent formation of SAMs on Au^{TS} surfaces by atomic force microscopy (AFM), spectroscopic ellipsometry, room-temperature scanning tunneling microscopy (STM), and X-ray photoelectron spectroscopy (XPS); see the Supporting Information for details. We completed the formation of Au^{TS}/SAM//EGaIn MEJs (where "/" and "//" represent covalent and van der Waals interactions, respectively) by contacting the SAMs with sharp tips of EGaIn such that the complexes define the electrode-to-electrode distance and characterized the tunneling currents by biasing the tip and grounding Au^{TS} substrate. To gain insight into the electronic structure of the complexes, we performed density functional theory (DFT) simulations on minimized gas-phase geometries.

The tunneling current density–voltage ($J - V$) characteristics of the SAMs measured between 1.5 and −1.5 V, are shown in Figure 2A–D. Measurements of MEJs comprising PcH_2 served as a control and yielded a higher conductance than the PcLnOAc series, for which all Ln complexes exhibited similar current densities and no immediately obvious trend. The high conductance of PcH_2 can be explained by the small tunneling barrier that results in the molecule lying flat on the Au^{TS} surface.

The series of Ln-$\{V_{12}\}$ hybrids exhibited a clear asymmetry in the J–V curves and reduced conductance compared to those of PcLnOAc, PcLn-$\{V_{12}\}$, and $(PcLn)_2$-$\{V_{12}\}$. Despite their larger size, the PcLn-$\{V_{12}\}$ and $(PcLn)_2$-$\{V_{12}\}$ hybrids also yielded higher conductances than PcLnOAc. The identity of the lanthanide, however, led to no clear effect on the J–V properties. Given the differences across this series, particularly their radii, this counterintuitive observation suggests that the current-carrying transmission channels are localized on the Pc moiety; otherwise the type of Ln complex, the width of the tunneling barrier, and the change in the number of counterions that are commensurate with the change of the lanthanide metal center would have some effect on the J–V characteristics. This hypothesis is supported by the peculiar behavior of the $\{V_{12}\}$ series, for which the asymmetry of the J–V curves vary based on the Ln complex and yield lower conductances compared to the smaller PcLnOAc and the larger PcLn-$\{V_{12}\}$ and $(PcLn)_2$-$\{V_{12}\}$ complexes; it suggests that, in the absence of the Pc moiety, the effects of the lanthanide complex and the $\{V_{12}\}$ moiety become observable because the transmission channels are no longer localized on a single (Pc) ligand.

The asymmetry of J–V curves (Figure 2E–H) can be quantified by the ratio of current density (J) or current I) at the two bias polarities (eq 1). The resulting values of log $|R|$ are inherently normalized, allowing for the comparison of differences in similarities across MEJs that produce different magnitudes of J. Small magnitudes of asymmetry (log $|R| < 0.5$ at 1 V) are regularly observed in MEJs comprising aliphatic molecules, which lack accessible states and is ascribed to intrinsic asymmetries such as SAM/electrode and SAM// electrode interfaces and the work functions of the electrodes.[45]

$$\log|R| = \log\left(\frac{|J(+V)|}{|J(-V)|}\right) \quad (1)$$

All of the PcLnOAc J–V curves (Figure 2E) show a slightly increased tunneling current at positive bias (log $|R| > 0$). The variation of the magnitude of log $|R|$ is not significant; therefore, the identity of the lanthanide centers does not seem to have a substantial impact on the asymmetry of the J–V curves. The Ln-$\{V_{12}\}$ complexes, however, exhibit considerable variation (Figure 2F) and, indeed, show significant differences in asymmetry across different metal centers. Interestingly, Dy-$\{V_{12}\}$ is the only complex for which log $|R| < 0.0$, meaning that the bias at which J is highest in magnitude is reversed compared to the other complexes. PcLn-$\{V_{12}\}$ and $(PcLn)_2$-$\{V_{12}\}$ complexes (Figure 2G,H) show effectively perfectly symmetrical curves, with log $|R| \approx 0$ for the entire bias range; PcGd-$\{V_{12}\}$ and $(PcGd)_2$-$\{V_{12}\}$ exhibit slight asymmetry, with log $|R| < 0$ at $V > 1.25$ V. In our previous work, we presented the Dy-$\{V_{12}\}$ complex, which notably shows complex electron transfer dynamics between the lanthanide and $\{V_{12}\}$ moieties.[39] Combined with the aforementioned values of log $|R|$, we hypothesize that the presence of the Pc ligand coordinated to a lanthanide ion dominates the frontier orbital structure to the extent that electronic properties and electrical characteristics become insensitive to the identity—and even the presence of—the lanthanide.

The data from spectroscopic ellipsometry and STM and AFM data are consistent with the formation of monolayers. From the ellipsometry and AFM data, the higher thickness and roughness, respectively, correlate to the SAMs comprising sterically bulkier molecules, as summarized in Table S1. The STM images show individual molecular fingerprints in Figure S1 while the AFM scans, as shown in Figure S2, clearly show complete passivation of the gold surface. However, these techniques cannot resolve the orientations of the individual complexes with respect to the substrate. To prove this orientation and to gain further insight into the role of the Pc ligand, we performed near-edge X-ray absorption fine structure (NEXAFS) spectroscopy on the PcGd-$\{V_{12}\}$ and $(PcGd)_2$-$\{V_{12}\}$ complexes (see Section S3.5 and Figure S5 for details). While the PcGd-$\{V_{12}\}$ complexes showed no clear preference in orientation with respect to the Au substrate, the $(PcGd)_2$-$\{V_{12}\}$ complexes show a dependence on the incident angle of the X-ray incidence angle, which suggests the Pc ligands prefer to lie upright on the Au substrate. This result suggests a direct interaction between the $\{V_{12}\}$ and the Au^{TS} substrate. A similar interaction between the Au electrodes and polyoxometalate structure, specifically the tungsten-based polyoxometalates, as a contact geometry for molecular junctions, was theoretically investigated recently by Lapham et al.[8] In a MEJ, this orientation places the electrodes in contact with the edges of the Pc ligands (as depicted in Figure 1F) rather than lying flat, with the lobes of the p-orbitals pointing into the electrode surfaces. This arrangement can explain both the weak dependence of conductance on the identity of the lanthanide and the higher conductances of the PcLn-$\{V_{12}\}$ and $(PcLn)_2$-$\{V_{12}\}$ complexes relative to the complexes that lack Pc ligands,

https://doi.org/10.1021/acsanm.3c05021
ACS Appl. Nano Mater. 2023, 6, 22643–22650

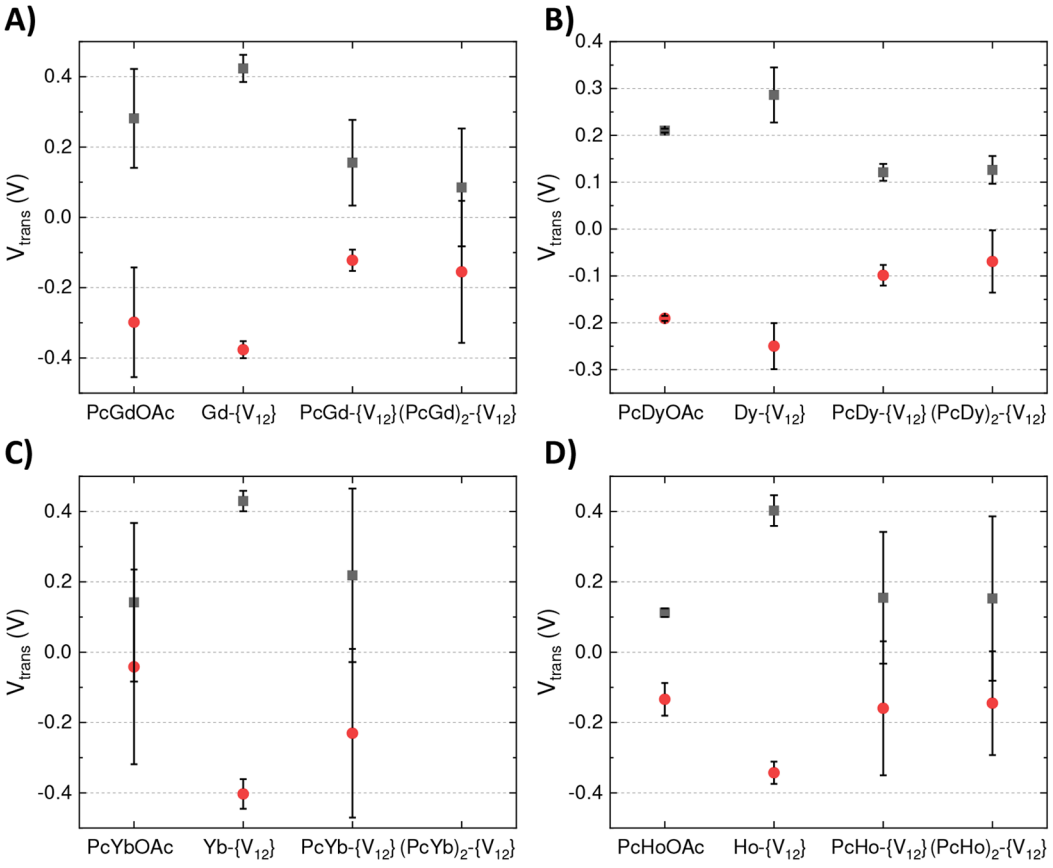

Figure 3. Transition voltages (V_{trans}) for positive (black) and negative (red) bias range, for the molecules under study, comprising the lanthanides Gd (A), Dy (B), Yb (C), and Pc (D). All complexes show similar values of V_{trans} when Pc is included and a clear increase in magnitude when it is omitted. Error bars represent 95% confidence intervals.

i.e., the $\{V_{12}\}$ and Ln-$\{V_{12}\}$. Direct contact to the Pc ligands favors charge transport through the π-conjugated pathways of the ligands, while in the absence of Pc, the Ln-$\{V_{12}\}$ complexes behave completely differently; the $J-V$ characteristics clearly depend on the identity of the lanthanide. Thus, Ln-$\{V_{12}\}$ complexes show promise for applications that seek to exploit the bonding and electronic structure of lanthanide cations, while the inclusion of Pc ligands creates transmission channels that are insensitive to the lanthanide. Given the breadth of the complexes we investigated, these results are unambiguous and provide a significant contribution toward the understanding of how to exploit the properties of f-block atoms and their interaction with the $\{V_{12}\}$ core, organic ligands, the surface, and the top (i.e., EGaIn) electrode.

To probe the $J-V$ characteristics further than magnitude and asymmetry, we extracted the transition voltages V_{trans}. Transition voltage spectroscopy has proven to be a very useful tool for understanding tunneling charge transport through MEJs by providing insight into the level alignment at bias.[46−48] In MEJs, V_{trans} is proportional to the energy offset between the tunneling transmission channel, which is usually a frontier molecular level, and the Fermi level (E_f) of the electrode.[47,49,50] As shown in Figure 3A, V_{trans} values (extracted from the $J-V$ data) at positive (black squares) and negative (red circles) bias are nearly symmetric, which is consistent with the $J-V$ data. For clarity, Figure 3 only shows data for complexes containing Gd, Dy, Yb, and Ho, all of which exhibit a clear trend, but different absolute values; data for all of the complexes are shown in Figure S11 along with a detailed explanation of the methodology used to extract V_{trans} in the Supporting Information. There is a clear trend in Figure 3 in which the magnitude of V_{trans} is lowest for PcLn-$\{V_{12}\}$ and $(PcLn)_2$-$\{V_{12}\}$ and highest for Ln-$\{V_{12}\}$, while the absolute values of V_{trans} are largest for Gd complexes and smallest for Ho complexes; however, the values of V_{trans} for the $(PcLn)_2$-$\{V_{12}\}$ complexes are nearly identical for the entire series (except $(PcYb)_2$-$\{V_{12}\}$ for which V_{trans} could not be reliably determined). Since the tunneling barrier is defined by the electronic state closest to E_f, the fact that V_{trans} is sensitive to the identity of the lanthanide is strong evidence that the electronic states that define the barrier for all but the $(PcLn)_2$-$\{V_{12}\}$ complexes are mixing with the lanthanide. But, by the same reasoning, the insensitivity of the absolute value of V_{trans} to identify Ln in the $(PcLn)_2$-$\{V_{12}\}$ complexes (Figure S11) supports the hypothesis that the Pc ligands define the tunneling barrier for the reasons described above.

Regardless of the orientation of the complexes, one explanation for the decoupling of $J-V$ properties from molecular structure is that the mechanism of charge transport is thermally activated hopping instead of (nonresonant) tunneling. To probe the mechanism of charge transport, we performed variable-temperature $J-V$ measurements using EGaIn electrodes both in a cross-bar configuration (Figure S8) and as conical tips identical to those used for the room-temperature measurements (Figure S9). Neither method showed a dependence of I on T, and Arrhenius plots showed

https://doi.org/10.1021/acsanm.3c05021
ACS Appl. Nano Mater. 2023, 6, 22643−22650

no activation energy; see Supporting Information for details. These results strongly suggest coherent tunneling transport at low bias, i.e., the absence of thermally activated hopping. For the measured complexes, in this case, Gd-{V_{12}}, PcGd-{V_{12}}, and $(PcGd)_2$-{V_{12}}, J does not vary with temperature. Thus, explaining the trends in the conductance, rectification, and V_{trans} requires additional insight into the electronic structures of the complexes.

We used DFT to predict the gas-phase geometries and single-point energies with the Amsterdam Modeling Suite (AMS).[51] We optimized the geometries of the metal complexes in gas phase followed by frequency calculations (to verify the absence of any imaginary frequencies) using the GGA:BLYP functional and TZP (Triple ζ Slater-type orbitals with 1 polarization function) basis set for nonlanthanide atoms and TZ2P+ for lanthanides. We utilized one-component zeroth order regular approximation (ZORA) relativistic effects, consistent with previously reported studies performed using ADF in vacuum at 0 K.[52,53] The ZORA/TZ2P+ basis is nearly identical to TZ2P but provides a better description of the f-space for the lanthanides La−Yb: 4f functions instead of 3.[54] For all the open-shell molecular systems, we performed unrestricted DFT simulations.

We computed gas-phase geometries of PcLnOAc for Ln = Gd^{III}, Yb^{III}, Lu^{III}, and Y^{III} as a non-lanthanide reference complex. In these complexes, the states with different f occupations can be very close in energy, leading to multi-configurational ground states. Hence, the monodeterminantal Kohn−Sham wave functions provided by DFT may give unreliable results. For instance, Yb^{III} ($[Xe]4f^{13}$) has one unpaired electron in the 4f shell and can occupy any one of the seven f orbitals. We performed single-point energy calculations on all seven possible configurations to identify the most probable ground state, as shown in Section S5.3. We compared the single-point energies of the seven structures and confirmed that the original electronic state was indeed the ground state for the PcYbOAc complex, with the total single-point energy of the next lowest state being 5.44 eV above the ground state. Thereafter, we performed spin-polarized unrestricted simulations with spin polarization of PcLnOAc complexes set to 7 and 1 for Gd and Yb, respectively, while spin−orbit effects were not accounted for. The plots for PcGdOAc and PcYbOAc are shown in the Supporting Information Figures S14−S17. The spin density (i.e., difference in the density of spin-up and spin-down) for PcGdOAc and PcYbOAc show that for PcGdOAc the spin is highly localized at the Gd^{III}, while for PcYbOAc the spin density is delocalized over Yb^{III} and the neighboring N atoms. These electronic structure properties of different Ln complexes are of potential interest for studies in molecular junctions; however, in our case, the supramolecular structure of the MEJs makes the experimental observations (J) insensitive to these electronic properties. Modifications to experimental platforms, such as in single-molecular junctions, conductive-probe atomic force microscopy setups, or magnetic field affected EGaIn MEJs could elucidate resulting spin effects in future studies on such Ln-containing complexes.

To make a qualitative comparison between our hypotheses based on the aforementioned experiments and the simulation results for the four types of complexes that we examined, we computed ground-state geometries for Lu^{III}-containing complexes. Since Lu^{III} has an electronic configuration of $[Xe]4f^{14}$, the simulations are more reliable owing to the monoconfigurational nature of the fully filled 4f-shell of the metal center. The highest occupied molecular orbital (HOMO) and lowest unoccupied molecular orbital (LUMO) are plotted in Figure 4.

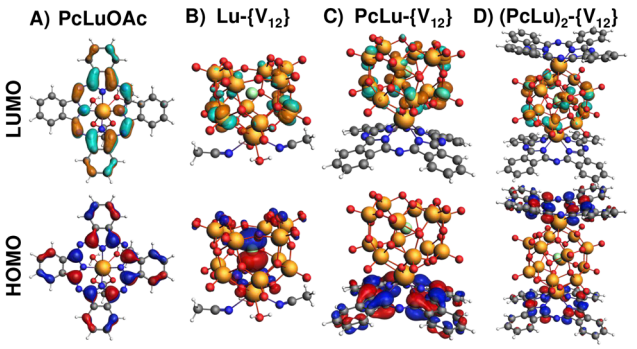

Figure 4. Plots of DFT-computed LUMO (top row, teal and purple) and HOMO (bottom row, red and blue) for the Lu complexes investigated in this work: (A) PcLuOAc, (B) Lu-{V_{12}}, (C) PcLu-{V_{12}}, and (D) $(PcLu)_2$-{V_{12}} and PcGdOAc. The plots of molecular orbitals for the Lu-{V_{12}}, PcLu-{V_{12}}, and $(PcLu)_2$-{V_{12}} complexes along with their corresponding counter cations are shown in Supporting Information Figure S18. We used isovalues of 0.02 to create these orbital plots.

We also ran similar calculations in the presence of tetramethylammonium counter cations for the Ln-{V_{12}}, PcLn-{V_{12}}, and $(PcLn)_2$-{V_{12}} complexes to have a charge-neutral molecular system and more physically realistic energy level values, which are provided in Table 1 and plotted in

Table 1. DFT Calculated Gas-Phase Energies of the Frontier Orbitals (eV) of the Four Complexes with Lu as the Metal Center.[a]

Molecular Orbital	PcLuOAc	Lu-{V_{12}}	PcLu-{V_{12}}	$(PcLu)_2$-{V_{12}}
HOMO	−4.66	−5.78	−3.90	−4.24
LUMO	−3.26	−4.33	−3.71	−4.20

[a]Two, four, and three tetramethylammonium countercations were included in the calculations for Lu-{V_{12}}, PcLu-{V_{12}}, and $(PcLu)_2$-{V_{12}}, respectively.

Figure S18. The HOMO and LUMO are delocalized on the Pc ligand for PcH_2 and PcLnOAc, while for PcLn-{V_{12}} and $(PcLn)_2$-{V_{12}} complexes, the HOMO and LUMO are localized on the Pc and the {V_{12}} moieties, respectively (Figure 4A,C,D). This orbital localization of the levels active in the electron transport window further hints toward strong intramolecular electronic interactions between the Pc and the {V_{12}} components, in agreement with our previous work on similar complexes in solution and solid state.[39] The orientation of the $(PcGd)_2$-{V_{12}} complexes places the Pc ligand in direct contact with the electrodes, suggesting that transport is HOMO-mediated in the PcLn-{V_{12}} and $(PcLn)_2$-{V_{12}} series. Furthermore, in the case of the Lu-{V_{12}} complex—for which the POV cage must be in contact with the electrodes—the HOMO lies on the metal center, while the LUMO is delocalized on the {V_{12}} cage. The presence of frontier orbitals present in the tunneling barrier on Pc in simulations of all the complexes except Ln-{V_{12}} supports our hypothesis that the tunneling charge transport is dominated by the Pc−lanthanide interaction; i.e., that the tunneling transmission channels are localized on the Pc ligand and only weakly influenced by the identity of the lanthanide. The presence of

https://doi.org/10.1021/acsanm.3c05021
ACS Appl. Nano Mater. 2023, 6, 22643−22650

high-lying levels (that contribute to the tunneling barrier) on the Pc in all of the PcLnOAc, PcLn-{V_{12}}, and $(PcL,n)_2$-{V_{12}} complexes explain the consistent magnitudes of J and V_{trans} and the distinct behavior of the Ln-{V_{12}} series.

CONCLUSIONS AND OUTLOOK

We examined an extensive and systematic series of lanthanide-functionalized polyoxovanadates, their related macrocyclic lanthanide complexes, and attendant controls in large-area MEJs to evaluate the potential of f-block elements in molecular-electronic devices. The polyoxovanadate-lanthanide-phtalocyanine hybrid complexes, $(PcLn)_n$-{V_{12}}, that we investigated exploit the responsive metal−ligand interaction resulting in electronically tunable molecular structures that readily form robust self-assembled monolayers. This robustness enabled a careful study of a large series of complexes, revealing what we postulate is the shielding of the 4f orbitals in the lanthanide metal centers by the phthalocyanine ligands due to weak metal−ligand interactions in lanthanide. The empirical result is a consistent trend in transition voltages (an approximation of the level-alignment at bias) and the vanishing effects from the identity of the lanthanide when two Pc ligands are present. We found that the mixing of the lanthanide and ligand states tends to dominate the transport levels, but we postulate that this observation is the result of how the complexes pack in molecular ensemble junctions; when the ligands bridge the two electrodes, they dominate transport and mask the effects of the lanthanide.

According to NEXAFS spectra, Pc ligands induce an edge-on orientation with the electrodes, particularly for the $(PcLn)_2$-{V_{12}} complexes. DFT calculations on gas-phase geometries suggest that the HOMO and LUMO localize on the Pc and POV ligands, respectively; thus the complexes that show a dependence on the identity of the lanthanide place the LUMO in contact with at least one electrode, while those that do not show the dependence place the HOMO in contact with at least one electrode. Thus, the spatial separation of the orbitals combined with the unique geometry of the complexes effectively selects spatial and electronic transport channels via the self-assembly process. And, unlike single-molecule junctions, these are static assemblies measured in device-relevant platforms. These observations predict potentially interesting effects for complexes that place the HOMO in contact with one electrode and the LUMO in contact with the other; however, the PcLn-{V_{12}} series shows no preferential orientation, averaging out any potential effect. Nonetheless, these preliminary DFT results naturally lead to further theoretical investigation on the electronic properties of these molecules when in contact with metal electrodes, as the alignment of molecular levels can be certainly affected by hybridization with the metal electrode. This study suggests at least three useful features of lanthanide complexes:

- Lanthanide complexes can serve as frameworks for including ligands in robust junctions in which the ligand can be tailored to affect the electrical characteristics of a junction without disturbing the self-assembly;
- because the electronic and spin states are delocalized, but frontier orbitals tend to localize on the ligands, spin and electronic structure can be used to impart potentially unique electrical properties in molecular-electronic junctions by designing ligands that place those states closest to the Fermi level. With further tuning of molecular design, for instance, by introducing aliphatic spacers, these levels can be decoupled from the electrodes to enhance the effect of redox properties on tunneling electrons;
- the class of ligands investigated in this study can be used to tune the geometry and self-assembly of the complexes for applications in mixed monolayers, specialized nanogap junctions formed from electrodes other than EGaIn and noble metals, etc.

Ultimately, this study opens pathways for investigating spin state induced electronic effects in molecular-electronic devices due to the high-spin configuration of the lanthanide metal centers, in combination with redox-active POV ligands, because they readily form robust junctions in high yields. The challenge going forward is utilizing the physical separation of the HOMO, LUMO, and spin between the ligands and lanthanide centers through functionalization to change the geometry, properties, and, hence, the electrical properties.

ASSOCIATED CONTENT

Supporting Information

The Supporting Information is available free of charge at https://pubs.acs.org/doi/10.1021/acsanm.3c05021.

Materials and methods, details of SAM formation and characterization, additional details of electrical measurements, and computational methods (PDF)

AUTHOR INFORMATION

Corresponding Authors

Kirill Yu. Monakhov − *Leibniz Institute of Surface Engineering (IOM), 04318 Leipzig, Germany;* orcid.org/0000-0002-1013-0680; Email: kirill.monakhov@iom-leipzig.de

Ryan C. Chiechi − *Department of Chemistry & Organic and Carbon Electronics Cluster, North Carolina State University, Raleigh, North Carolina 27695-8204, United States;* orcid.org/0000-0002-0895-2095; Email: ryan.chiechi@ncsu.edu

Authors

Saurabh Soni − *Stratingh Institute for Chemistry, University of Groningen, 9747 AG Groningen, The Netherlands; Zernike Institute for Advanced Materials, 9747 AG Groningen, The Netherlands;* Present Address: Hybrid Materials for Optoelectronics Group, Department of Molecules and Materials, MESA+ Institute for Nanotechnology, Molecules Center and Center for Brain-Inspired Nano Systems, Faculty of Science and Technology, University of Twente, P.O. Box 2017, 7500 AE Enschede, The Netherlands; orcid.org/0000-0002-8159-9128

Irina Werner − *Leibniz Institute of Surface Engineering (IOM), 04318 Leipzig, Germany*

Michael Aidi − *Stratingh Institute for Chemistry, University of Groningen, 9747 AG Groningen, The Netherlands; Zernike Institute for Advanced Materials, 9747 AG Groningen, The Netherlands*

Marco Moors − *Leibniz Institute of Surface Engineering (IOM), 04318 Leipzig, Germany;* orcid.org/0000-0002-3340-9756

C. Lungani Mthembu − *Stratingh Institute for Chemistry, University of Groningen, 9747 AG Groningen, The*

https://doi.org/10.1021/acsanm.3c05021
ACS Appl. Nano Mater. 2023, 6, 22643−22650

Netherlands; Zernike Institute for Advanced Materials, 9747 AG Groningen, The Netherlands

Michael Zharnikov − *Applied Physical Chemistry, Heidelberg University, D-69120 Heidelberg, Germany*

Remco W. A. Havenith − *Stratingh Institute for Chemistry, University of Groningen, 9747 AG Groningen, The Netherlands; Zernike Institute for Advanced Materials, 9747 AG Groningen, The Netherlands; Department of Chemistry, Ghent University, B-9000 Ghent, Belgium;* orcid.org/0000-0003-0038-6030

Complete contact information is available at: https://pubs.acs.org/10.1021/acsanm.3c05021

Notes

The authors declare no competing financial interest.

■ ACKNOWLEDGMENTS

We thank the Center for Information Technology of the University of Groningen for their support and for providing access to the Peregrine high performance computing cluster. S.S. acknowledges the Zernike Institute for Advanced Materials. We thank NWO for access to the Dutch national e-infrastructure (Cartesius) with the support of SURF Cooperative on which part of this work was carried out. M.Z. thanks the Helmholtz Zentrum Berlin for the allocation of synchrotron radiation beamtime at BESSY II and Yangbiao Liu for the assistance at the evaluation of the NEXAFS data. This work was supported by the Deutsche Forschungsgemeinschaft (DFG) project number 432224404.

■ REFERENCES

(1) Vilan, A.; Aswal, D.; Cahen, D. Large-Area, Ensemble Molecular Electronics: Motivation and Challenges. *Chem. Rev.* **2017**, *117*, 4248−4286.

(2) Liu, Y.; Qiu, X.; Soni, S.; Chiechi, R. C. Charge Transport Through Molecular Ensembles: Recent Progress in Molecular Electronics. *Chem. Phys. Rev.* **2021**, *2*, 021303.

(3) Zhao, Z.; Soni, S.; Lee, T.; Nijhuis, C. A.; Xiang, D. Smart Eutectic Gallium−Indium: From Properties to Applications. *Adv. Mater.* **2023**, *35*, 2203391.

(4) Laurans, M.; Dalla Francesca, K.; Volatron, F.; Izzet, G.; Guerin, D.; Vuillaume, D.; Lenfant, S.; Proust, A. Molecular Signature of Polyoxometalates in Electron Transport of Silicon-Based Molecular Junctions. *Nanoscale* **2018**, *10*, 17156−17165.

(5) Huez, C.; Guérin, D.; Lenfant, S.; Volatron, F.; Calame, M.; Perrin, M. L.; Proust, A.; Vuillaume, D. Redox-Controlled Conductance of Polyoxometalate Molecular Junctions. *Nanoscale* **2022**, *14*, 13790−13800.

(6) Moors, M.; Warneke, J.; López, X.; de Graaf, C.; Abel, B.; Monakhov, K. Y. Insights From Adsorption and Electron Modification Studies of Polyoxometalates on Surfaces for Molecular Memory Applications. *Acc. Chem. Res.* **2021**, *54*, 3377−3389.

(7) Kondinski, A.; Ghorbani-Asl, M. Polyoxoplatinates as Covalently Dynamic Electron Sponges and Molecular Electronics Materials. *Nanoscale Advances* **2021**, *3*, 5663−5675.

(8) Lapham, P.; Vilà-Nadal, L.; Cronin, L.; Georgiev, V. P. Influence of the Contact Geometry and Counterions on the Current Flow and Charge Transfer in Polyoxometalate Molecular Junctions: A Density Functional Theory Study. *J. Phys. Chem. C* **2021**, *125*, 3599−3610.

(9) Laurans, M.; Trinh, K.; Dalla Francesca, K.; Izzet, G.; Alves, S.; Derat, E.; Humblot, V.; Pluchery, O.; Vuillaume, D.; Lenfant, S.; Volatron, F.; Proust, A. Covalent Grafting of Polyoxometalate Hybrids Onto Flat Silicon/Silicon Oxide: Insights From POMs Layers on Oxides. *ACS Appl. Mater. Interfaces* **2020**, *12*, 48109−48123.

(10) Raj, G.; Swalus, C.; Arendt, E.; Eloy, P.; Devillers, M.; Gaigneaux, E. M. Controlling the Dispersion of Supported Polyoxometalate Heterogeneous Catalysts: Impact of Hybridization and the Role of Hydrophilicity-Hydrophobicity Balance and Supramolecularity. *Beilstein J. Nanotechnol.* **2014**, *5*, 1749−1759.

(11) Smith, T. The Hydrophilic Nature of a Clean Gold Surface. *J. Colloid Interface Sci.* **1980**, *75*, 51−55.

(12) Cherevan, A. S.; Nandan, S. P.; Roger, I.; Liu, R.; Streb, C.; Eder, D. Polyoxometalates on Functional Substrates: Concepts, Synergies, and Future Perspectives. *Adv. Sci.* **2020**, *7*, 1903511.

(13) Gunaratne, K. D. D.; Johnson, G. E.; Andersen, A.; Du, D.; Zhang, W.; Prabhakaran, V.; Lin, Y.; Laskin, J. Controlling the Charge State and Redox Properties of Supported Polyoxometalates via Soft Landing of Mass-Selected Ions. *J. Phys. Chem. C* **2014**, *118*, 27611−27622.

(14) Dalla Francesca, K.; Lenfant, S.; Laurans, M.; Volatron, F.; Izzet, G.; Humblot, V.; Methivier, C.; Guerin, D.; Proust, A.; Vuillaume, D. Charge Transport Through Redox Active $[H_7P_8W_{48}O_{184}]^{33-}$ Polyoxometalates Self-Assembled Onto Gold Surfaces and Gold Nanodots. *Nanoscale* **2019**, *11*, 1863−1878.

(15) Primera-Pedrozo, O. M.; Tan, S.; Zhang, D.; O'Callahan, B. T.; Cao, W.; Baxter, E. T.; Wang, X.-B.; El-Khoury, P. Z.; Prabhakaran, V.; Glezakou, V.-A.; Johnson, G. E. Influence of Surface and Intermolecular Interactions on the Properties of Supported Polyoxometalates. *Nanoscale* **2023**, *15*, 5786−5797.

(16) Vogelsberg, E.; Moors, M.; Sorokina, A. S.; Ryndyk, D. A.; Schmitz, S.; Freitag, J. S.; Subbotina, A. V.; Heine, T.; Abel, B.; Monakhov, K. Y. Solution-Processed Formation of DNA-Origami-Supported Polyoxometalate Multi-Level Switches With Counter-cation-Controlled Conductance Tunability. *Chem. Mater.* **2023**, *35*, 5447−5457.

(17) Gillet, A.; Cher, S.; Tassé, M.; Blon, T.; Alves, S.; Izzet, G.; Chaudret, B.; Proust, A.; Demont, P.; Volatron, F.; Tricard, S. Polarizability Is a Key Parameter for Molecular Electronics. *Nano. Horiz.* **2021**, *6*, 271−276.

(18) Cinchetti, M.; Dediu, V. A.; Hueso, L. E. Activating the Molecular Spinterface. *Nat. Mater.* **2017**, *16*, 507−515.

(19) Fahrendorf, S.; Atodiresei, N.; Besson, C.; Caciuc, V.; Matthes, F.; Blügel, S.; Kögerler, P.; Bürgler, D. E.; Schneider, C. M. Accessing 4f-States in Single-Molecule Spintronics. *Nat. Commun.* **2013**, *4*, 2425.

(20) van de Burgt, Y.; Melianas, A.; Keene, S. T.; Malliaras, G.; Salleo, A. Organic Electronics for Neuromorphic Computing. *Nat. Electron.* **2018**, *1*, 386−397.

(21) Zhang, Y.; Liu, L.; Tu, B.; Cui, B.; Guo, J.; Zhao, X.; Wang, J.; Yan, Y. An Artificial Synapse Based on Molecular Junctions. *Nat. Commun.* **2023**, *14*, 247.

(22) Wang, Y.; Zhang, Q.; Astier, H. P. A. G.; Nickle, C.; Soni, S.; Alami, F. A.; Borrini, A.; Zhang, Z.; Honnigfort, C.; Braunschweig, B.; Leoncini, A.; Qi, D.-C.; Han, Y.; del Barco, E.; Thompson, D.; Nijhuis, C. A. Dynamic Molecular Switches With Hysteretic Negative Differential Conductance Emulating Synaptic Behaviour. *Nat. Mater.* **2022**, *21*, 1403−1411.

(23) Park, S.; Yoon, H. J. Thermal and Thermoelectric Properties of SAM-Based Molecular Junctions. *ACS Appl. Mater. Interfaces* **2022**, *14*, 22818−22825.

(24) Clemente-Juan, J. M.; Coronado, E.; Gaita-Ariño, A. Magnetic Polyoxometalates: From Molecular Magnetism to Molecular Spintronics and Quantum Computing. *Chem. Soc. Rev.* **2012**, *41*, 7464.

(25) Duan, Y.; Rosaleny, L. E.; Coutinho, J. T.; Giménez-Santamarina, S.; Scheie, A.; Baldoví, J. J.; Cardona-Serra, S.; Gaita-Ariño, A. Data-Driven Design of Molecular Nanomagnets. *Nat. Commun.* **2022**, *13*, 7626.

(26) Fuller, C. W.; Padayatti, P. S.; Abderrahim, H.; Adamiak, L.; Alagar, N.; Ananthapadmanabhan, N.; Baek, J.; Chinni, S.; Choi, C.; Delaney, K. J.; Dubielzig, R.; Frkanec, J.; Garcia, C.; Gardner, C.; Gebhardt, D.; Geiser, T.; Gutierrez, Z.; Hall, D. A.; Hodges, A. P.; Hou, G.; Jain, S.; Jones, T.; Lobaton, R.; Majzik, Z.; Marte, A.; Mohan, P.; Mola, P.; Mudondo, P.; Mullinix, J.; Nguyen, T.; Ollinger,

F.; Orr, S.; Ouyang, Y.; Pan, P.; Park, N.; Porras, D.; Prabhu, K.; Reese, C.; Ruel, T.; Sauerbrey, T.; Sawyer, J. R.; Sinha, P.; Tu, J.; Venkatesh, A. G.; VijayKumar, S.; Zheng, L.; Jin, S.; Tour, J. M.; Church, G. M.; Mola, P. W.; Merriman, B. Molecular Electronics Sensors on a Scalable Semiconductor Chip: A Platform for Single-Molecule Measurement of Binding Kinetics and Enzyme Activity. *Proc. Natl. Acad. Sci. U. S. A.* **2022**, *119*, e2112812119.

(27) Kos, D.; Di Martino, G.; Boehmke, A.; de Nijs, B.; Berta, D.; Foldes, T.; Sangtarash, S.; Rosta, E.; Sadeghi, H.; Baumberg, J. J. Optical Probes of Molecules as Nano-Mechanical Switches. *Nat. Commun.* **2020**, *11*, 5905.

(28) Wang, M.; Wang, T.; Ojambati, O. S.; Duffin, T. J.; Kang, K.; Lee, T.; Scheer, E.; Xiang, D.; Nijhuis, C. A. Plasmonic Phenomena in Molecular Junctions: Principles and Applications. *Nat. Rev. Chem.* **2022**, *6*, 681−704.

(29) Yi, X.; Izarova, N. V.; Stuckart, M.; Guérin, D.; Thomas, L.; Lenfant, S.; Vuillaume, D.; van Leusen, J.; Duchoň, T.; Nemšák, S.; Bourone, S. D. M.; Schmitz, S.; Kögerler, P. Probing Frontier Orbital Energies of {Co9(P2W15)3} Polyoxometalate Clusters at Molecule-Metal and Molecule-Water Interfaces. *J. Am. Chem. Soc.* **2017**, *139*, 14501−14510.

(30) AlDamen, M. A.; Clemente-Juan, J. M.; Coronado, E.; Martí-Gastaldo, C.; Gaita-Ariño, A. Mononuclear Lanthanide Single-Molecule Magnets Based on Polyoxometalates. *J. Am. Chem. Soc.* **2008**, *130*, 8874−8875.

(31) Baldoví, J. J.; Duan, Y.; Bustos, C.; Cardona-Serra, S.; Gouzerh, P.; Villanneau, R.; Gontard, G.; Clemente-Juan, J. M.; Gaita-Ariño, A.; Giménez-Saiz, C.; Proust, A.; Coronado, E. Single Ion Magnets Based on Lanthanoid Polyoxomolybdate Complexes. *Dalton Trans.* **2016**, *45*, 16653−16660.

(32) Boskovic, C. Rare Earth Polyoxometalates. *Acc. Chem. Res.* **2017**, *50*, 2205−2214.

(33) Ritchie, C.; Baslon, V.; Moore, E. G.; Reber, C.; Boskovic, C. Sensitization of Lanthanoid Luminescence by Organic and Inorganic Ligands in Lanthanoid-Organic-Polyoxometalates. *Inorg. Chem.* **2012**, *51*, 1142−1151.

(34) Mougharbel, A. S.; Bhattacharya, S.; Bassil, B. S.; Rubab, A.; van Leusen, J.; Kögerler, P.; Wojciechowski, J.; Kortz, U. Lanthanide-Containing 22-Tungsto-2-Germanates $[Ln(GeW_{11}O_{39})_2]^{13-}$: Synthesis, Structure, and Magnetic Properties. *Inorg. Chem.* **2020**, *59*, 4340−4348.

(35) Yang, W.; Li, X.; Chi, D.; Zhang, H.; Liu, X. Lanthanide-Doped Upconversion Materials: Emerging Applications for Photovoltaics and Photocatalysis. *Nanotechnology* **2014**, *25*, 482001.

(36) Pütt, R.; Qiu, X.; Kozłowski, P.; Gildenast, H.; Linnenberg, O.; Zahn, S.; Chiechi, R. C.; Monakhov, K. Y. Self-Assembled Monolayers of Polyoxovanadates With Phthalocyaninato Lanthanide Moieties on Gold Surfaces. *Chem. Commun.* **2019**, *55*, 13554−13557.

(37) Weiss, E. A.; Kaufman, G. K.; Kriebel, J. K.; Li, Z.; Schalek, R.; Whitesides, G. M. Si/SiO2-Templated Formation of Ultraflat Metal Surfaces on Glass, Polymer, and Solder Supports: Their Use as Substrates for Self-Assembled Monolayers. *Langmuir* **2007**, *23*, 9686−9694.

(38) Chiechi, R. C.; Weiss, E. A.; Dickey, M. D.; Whitesides, G. M. Eutectic Gallium-Indium (EGaIn): A Moldable Liquid Metal for Electrical Characterization of Self-Assembled Monolayers. *Angew. Chem., Int. Ed.* **2008**, *47*, 142−144.

(39) Werner, I.; Griebel, J.; Masip-Sánchez, A.; López, X.; Załęski, K.; Kozłowski, P.; Kahnt, A.; Boerner, M.; Warneke, Z.; Warneke, J.; Monakhov, K. Y. Hybrid Molecular Magnets With Lanthanide- And Countercation-Mediated Interfacial Electron Transfer Between Phthalocyanine and Polyoxovanadate. *Inorg. Chem.* **2023**, *62*, 3761−3775.

(40) Monakhov, K. Y. Implication of Counter-Cations for Polyoxometalate-Based Nano-Electronics. *Comments Inorg. Chem.* **2022**, 1−10.

(41) Sorokina, A. S.; Ryndyk, D. A.; Monakhov, K. Y.; Heine, T. What Is the Maximum Charge Uptake of Lindqvist-Type Polyoxovanadates in Organic-Inorganic Heterostructures? *Phys. Chem. Chem. Phys.* **2022**, *24*, 26848−26852.

(42) Bouvet, M.; Bassoul, P.; Simon, J. Synthesis and Electrical Properties of a New Molecular Semiconductor: The Unsymmetrical Lutetium Phthalo-Naphthalocyanine. *Mol. Cryst. Liq. Cryst.* **1994**, *252*, 31−38.

(43) Okaya, K.; Kobayashi, T.; Koyama, Y.; Hayashi, Y.; Isobe, K. Formation of V^v Lacunary Polyoxovanadates and Interconversion Reactions of Dodecavanadate Species. *Eur. J. Inorg. Chem.* **2009**, *2009*, 5156−5163.

(44) Cameron, J. M.; Newton, G. N.; Busche, C.; Long, D.-L.; Oshio, H.; Cronin, L. Synthesis and Characterisation of a Lanthanide-Capped Dodecavanadate Cage. *Chem. Commun.* **2013**, *49*, 3395.

(45) Zhang, Y.; Soni, S.; Krijger, T. L.; Gordiichuk, P.; Qiu, X.; Ye, G.; Jonkman, H. T.; Herrmann, A.; Zojer, K.; Zojer, E.; Chiechi, R. C. Tunneling Probability Increases with Distance in Junctions Comprising Self-Assembled Monolayers of Oligothiophenes. *J. Am. Chem. Soc.* **2018**, *140*, 15048−15055.

(46) Xie, Z.; Bâldea, I.; Smith, C. E.; Wu, Y.; Frisbie, C. D. Experimental and Theoretical Analysis of Nanotransport in Oligophenylene Dithiol Junctions as a Function of Molecular Length and Contact Work Function. *ACS Nano* **2015**, *9*, 8022−8036.

(47) Bâldea, I. Ambipolar Transition Voltage Spectroscopy: Analytical Results and Experimental Agreement. *Phys. Rev. B* **2012**, *85*, 035442.

(48) Carlotti, M.; Soni, S.; Kovalchuk, A.; Kumar, S.; Hofmann, S.; Chiechi, R. C. Empirical Parameter to Compare Molecule−Electrode Interfaces in Large-Area Molecular Junctions. *ACS Phys. Chem. Au* **2022**, *2*, 179−190.

(49) Beebe, J. M.; Kim, B.; Frisbie, C. D.; Kushmerick, J. G. Measuring Relative Barrier Heights in Molecular Electronic Junctions With Transition Voltage Spectroscopy. *ACS Nano* **2008**, *2*, 827−832.

(50) Zhang, Y.; Qiu, X.; Gordiichuk, P.; Soni, S.; Krijger, T. L.; Herrmann, A.; Chiechi, R. C. Mechanically and Electrically Robust Self-Assembled Monolayers for Large-Area Tunneling Junctions. *J. Phys. Chem. C* **2017**, *121*, 14920−14928.

(51) *ADF 2019.3*; SCM, Theoretical Chemistry, Vrije Universiteit: Amsterdam, The Netherlands, 2019; http://www.scm.com.

(52) Roy, L. E.; Hughbanks, T. Magnetic Coupling in Dinuclear Gd Complexes. *J. Am. Chem. Soc.* **2006**, *128*, 568−575.

(53) Yazyev, O. V.; Helm, L. O17 Nuclear Quadrupole Coupling Constants of Water Bound to a Metal Ion: A Gadolinium(III) Case Study. *J. Chem. Phys.* **2006**, *125*, 054503.

(54) Chong, D. P.; Van Lenthe, E.; Van Gisbergen, S.; Baerends, E. J. Even-Tempered Slater-Type Orbitals Revisited: From Hydrogen to Krypton. *J. Comput. Chem.* **2004**, *25*, 1030−1036.

https://doi.org/10.1021/acsanm.3c05021
ACS Appl. Nano Mater. 2023, 6, 22643−22650